A Dual-Signal Electrochemiluminescence Sensor for Kanamycin Detection Based on Self-Enhanced Zr MOFs and Single Co-Reactant Competition Mechanism

Yawen Zhu , Xuemei Wang , Zhiyong Yan , Feifei Zhang , Jianfei Xia , Lili Lv * , Zonghua Wang *

Posted Date: 10 April 2025

doi: 10.20944/preprints202504.0813.v1

Keywords: self-enhanced electrochemiluminescence; competitive; dual-signal; metal-organic framework; luminol; kanamycin

 doi:10.20944/preprints202504.0813.v1

Article

A Dual-Signal Electrochemiluminescence Sensor for Kanamycin Detection Based on Self-Enhanced Zr MOFs and Single Co-Reactant Competition Mechanism

Yawen Zhu [1,†], Xuemei Wang [1,†], Zhiyong Yan [2], Feifei Zhang [1], Jianfei Xia [1], Lili Lv [1,*] and Zonghua Wang [1,3,*]

[1] College of Chemistry and Chemical Engineering, Instrumental Analysis Center of Qingdao University, College of Materials Science and Engineering, Qingdao Application Technology Innovation Center of Photoelectric Biosensing for Clinical Diagnosis and Treatment, Shandong Sino-Japanese Center for Collaborative Research of Carbon Nanomaterials, Qingdao University, Qingdao 266071, China

[2] Institute of Analysis and Testing, Beijing Academy of Science and Technology (Beijing Center for Physical and Chemical Analysis), Beijing 100089, China

[3] Characteristic Laboratory of Advanced Metal Functional Materials and Processing in Universities of Shandong, School of Mechanical and Electronic Engineering, Qingdao Binhai University, Qingdao 266555, China

* Correspondence: lvll@qdu.edu.cn (L.L.); wangzonghua@qdu.edu.cn (Z.W.); Tel.: +86-1385-321-9173 (Z.W.)

† These authors contributed equally to this work.

Abstract: The dual-signal output self-calibration mode reduces false positive or negative signals of electrochemiluminescence (ECL) aptamer sensors. A competitive dual-signal ECL platform was designed for ultrasensitive detection of kanamycin (KAN)using zirconium metal-organic frameworks (Zr MOFs) and Luminol as ECL emitters. To enhance the ECL efficiency, co-reactant (polyethyleneimine, PEI) was covalently bound to Zr MOFs to achieve the self-enhanced ECL. Based on the selective interaction between KAN and its aptamer, the Luminol/KAN/Zr MOFs-PEI "sandwich" structure was immobilized on the electrode surface. The competition for PEI between emitters increased the Luminol ECL signal and decreased the Zr MOFs ECL signal. The ratio in ECL signals between the two competitive emitters enabled the quantitative analysis of KAN, achieving a detection limit as low as 7.86×10^{-4} ng/mL. This study elucidated the synergistic mechanism between self-enhanced ECL and ECL competition, offering a novel approach for constructing dual-signal ECL sensors using a single co-reactant.

Keywords: self-enhanced electrochemiluminescence; competitive; dual-signal; metal-organic framework; luminol; kanamycin

1. Introduction

Kanamycin (KAN), a powerful inhibitor of protein synthesis, has been extensively used in medicine and as an additive in livestock feed [1,2]. However, the excessive use of KAN has resulted in significant accumulation in humans, aquatic environments, animals, and plants, thereby posing substantial challenges to health and environmental safety [3–5]. The European Union has implemented stringent regulations in an effort to raise public awareness about the adverse impacts (tinnitus, diarrhea, skin rashes and even fatalities in severe cases) of KAN residues to protect human health [6]. The maximum allowable residue limit (MRL) for KAN in milk should not exceed 100 μg/kg, while the MRL specified 200 μg/kg in Chinese regulation [7]. A variety of techniques, including colorimetry [8,9], fluorescence [10,11], UV−vis spectroscopy [12], photoelectrochemistry [13], electrochemistry [14,15], electrochemiluminescence [16] and so on, have been proposed for the

 doi:10.20944/preprints202504.0813.v1

detection of KAN in recent years. Among these methods, electrochemiluminescence (ECL) has garnered attention for its low signal background, high sensitivity, great controllability and rapid detection [17–19].

Normally, ECL detection was a single-signal model, which could easily lead to erroneous outcomes in complex detection environments. In comparison, employing the dual-signal output mode in ECL detection allows for effective error mitigation through self-calibration [20–23], thus improving the reliability and sensitivity of the sensor. For instance, Dai et al. [24] created europium-based organic gels (Eu-L-H MOGs) by employing europium ions as metal nodes and incorporating Luminol and 4'-(4-carboxyphenyl)-2,2':6',2″-terpyridine (Hcptpy) as ligands. Using dissolved oxygen and $K_2S_2O_8$ as co-reactants, high sensitivity detection of the I27L gene was achieved by comparing the anodic ECL signal of Luminol with the cathodic ECL signal of Hcptpy. It can be observed that, dual luminophores system generally requires the introduction of dual co-reactants, thereby unavoidably complicating the detection environment and impacting the accuracy of the results. Moreover, the inherent instability of exogenous co-reactants limits the widespread application of the ECL system. The self-enhanced ECL strategy presents a practical solution to these issues. Through the covalent bonding of the co-reactant with the luminophore, not only substantially shortens the electron transport distance and improves ECL efficiency, but also effectively mitigates the interference in the detection environment, thus improving the accuracy of the analytical results. Therefore, identifying suitable luminophores and co-reactants is crucial in the development of dual-signal self-enhanced ECL sensing systems.

In recent years, the rapid development of materials science has promoted the continuous progress of ECL, and the emergence of various luminescent materials has provided a broad space for developing dual-signal ECL sensors. Metal-organic frameworks (MOFs) have shown significant potential [25–27]. These crystalline structures consist of metal ions or clusters self-assembled with organic ligands, possessing a distinctive porous structure and tunability, which have advantages in the construction of sensors. In particular, Zirconium-based MOFs (Zr MOFs) have garnered considerable attention due to their exceptional chemical stability and tunable porosity, and gradually occupied an important position in the construction of ECL sensors [28,29]. Compared with other nanomaterials, Zr MOFs exhibit superior chemical robustness under harsh environmental conditions, ensuring the long-term stability of the sensor. Additionally, the high surface area and abundant coordination sites of Zr MOFs provide ample space for co-reactant immobilization, thereby enhancing the interaction between luminophores and co-reactants. More importantly, the covalent coupling of PEI with Zr MOFs significantly shortens the electron transfer distance, which not only enhances the ECL efficiency but also reduces the interference of additional reagents in the detection environment. These features highlight the remarkable potential of Zr MOFs in constructing self-enhanced and competitive dual-signal ECL sensors.

In this work, Zr MOFs was chosen as one of the luminophores. To enhance the ECL performance of Zr MOFs, the co-reactant (polyethyleneimine, PEI) was covalently bonded to Zr MOFs to form Zr MOFs-PEI composite, which produced an intramolecular self-enhancement effect. Luminol, as one of the most classic luminophore [30–32], has the advantages of low cost, good water solubility and low excitation potential. It has a high and stable ECL emission efficiency with the presence of the PEI, thus it was selected as an additional luminophore. Based on the competition between Luminol and Zr MOFs for PEI, appropriate amount of PEI was covalently linked to Zr MOFs, and the synergistic effect of self-enhancing strategy and competition mechanism was discussed, so as to conduct accurate quantitative analysis of the target. This is crucial for the successful construction of competitive dual-signal ECL sensors.

Herein, an innovative dual-signal ECL aptamer sensor was developed for KAN detection, leveraging the competition between Zr MOFs and Luminol for the same co-reactant, as illustrated in Scheme 1. The KAN's aptamer specifically recognized KAN and acted as a bridge between Zr MOFs-PEI and Luminol at the nanoscale to form a "sandwich" structure. The competition for PEI between the two emitters resulted in an increase of Luminol ECL signal and a decrease of Zr MOFs ECL signal.

 doi:10.20944/preprints202504.0813.v1

As a result, the constructed competitive dual-signal ECL aptamer sensor exhibits excellent sensitivity, accuracy, and promising potential for real sample analysis.

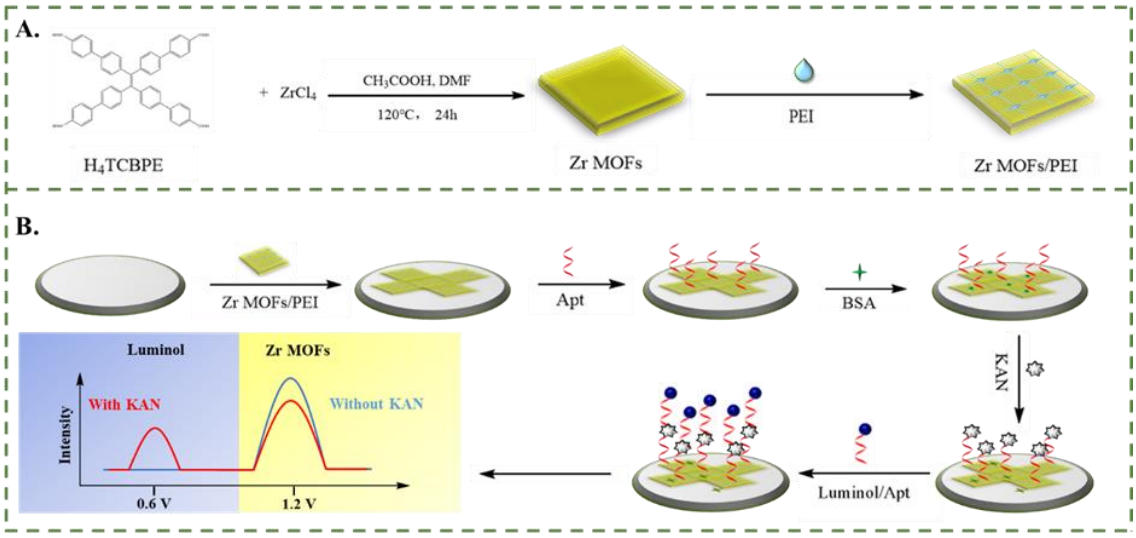

Scheme 1. Schematic illustration for (A) the preparation of Zr MOFs-PEI composite, (B) the fabrication process of the competitive dual-signal ECL aptamer sensor.

2. Experimental Section

The materials and reagents can be found in the Supplementary Materials.

2.1. Preparation of Zr MOFs and Zr MOFs-PEI Composite

60 mg of $ZrCl_4$, 30 mg of H_4TCBPE, and 1 mL of CH_3COOH were ultrasonically dissolved in 15 mL of DMF, followed by heating at 120℃ for 24 h. After cooling down to room temperature, the product was washed thrice with ethanol and water. Subsequently, the precipitate was centrifuged and dried under vacuum at 60℃ overnight, yielding a pale yellow powder suitable for subsequent research.

Subsequently, 1 mL of Zr MOFs (1 mg/mL) was combined with 200 μL of EDC (0.4 M) and NHS (0.1 M) under magnetic stirring for 1.5 h. Next, 500 μL of PEI (1%) was added dropwise and stirred continuously overnight. The prepared Zr MOFs-PEI was centrifuged at 11000 rpm for 5 min, and the sediment was washed thrice, redispersed in 1 mL of ultrapure water, and stored at 4℃ for later use.

2.2. Preparation of Luminol-Apt

The synthesis of Luminol-Apt process can be found in the Supplementary Materials.

2.3. Preparation of ECL Aptamer Sensors

As shown in Scheme 1B, the glassy carbon electrode (GCE) was initially polished using Al_2O_3 powder and sonicated in anhydrous ethanol and ultrapure water later, eventually dried with nitrogen gas. 10 μL of Zr MOFs-PEI was then applied onto the pre-treated GCE and air-dry at 25℃. The obtained Zr MOFs-PEI/GCE surface was dropped with 10 μL of aptamer solution and incubated at 37℃ for 2 h. To minimize non-specific adsorption, the Apt/Zr MOFs-PEI/GCE was incubated with 0.5% BSA at 37℃ for 1 h. Following this, the Apt/Zr MOFs-PEI/GCE was immersed in KAN solution at 37°C for 1 h. Finally, the KAN/Apt/Zr MOFs-PEI/GCE was placed into Luminol-Apt solution and incubated at 37℃ for 2 h, the modified electrode was gently washed with PBS to obtain the ECL aptamer sensors (Luminol-Apt/KAN/Apt/Zr MOFs-PEI/GCE).

 doi:10.20944/preprints202504.0813.v1

3. Results and Discussion

3.1. Characterization of Zr MOFs and Zr MOFs-PEI

Firstly, the morphology of the synthesized materials was examined using scanning electron microscopy (SEM). As depicted in Figure 1A, the synthesized Zr MOFs exhibited a uniform cubic shape, averaging 800 nm in diameter. Due to the linkage of PEI, the previously smooth surface of Zr MOFs showed an obvious rough texture (Figure 1B). Meanwhile, the cubic morphology of Zr MOFs-PEI could also be observed by the transmission electron microscopy (TEM) image (Figure 1C). The elemental mapping image of Zr MOFs-PEI (Figure 1D) depicted a uniform distribution of Zr, C, O, and N elements, verifying that Zr MOFs-PEI composite was successfully prepared. The X-ray diffraction (XRD) pattern in Figure 1E revealed that the characteristic peaks of Zr MOFs were significantly consistent with those of the simulated pattern [33]. It proved that the synthesized Zr MOFs achieved the expected results. Figure 1F presented the UV-vis absorption spectrum of Zr MOFs, revealing a distinct absorption peak at 420 nm. The XPS spectra revealed the elemental composition and chemical states of the Zr-based MOFs. The full spectrum shown in Figure 1G indicated the presence of O, C and Zr elements. In Figure 1H, the O 1s peak split into two peaks at 529.7 eV and 531.0 eV, attributed to the oxo compounds of H_4TCBPE and the Zr-O bonds in the Zr MOFs. In Figure 1I, the C 1s spectrum displayed two distinct peaks at 284.1 eV and 288.4 eV, corresponding to the benzoic acid rings of the organic ligand H_4TCBPE and the C=O bonds, respectively. In the Zr 3d spectrum (Figure 1J), the peaks fitted at binding energies of 181.8 eV and 184.2 eV attribute to Zr $3d_{5/2}$ and Zr $3d_{3/2}$, respectively, confirming the presence of Zr (IV). These XPS results supported the formation of the MOFs. Figure S1 depicted the Fourier transform infrared (FT-IR) spectral image of Zr MOFs and Zr MOFs-PEI. Compared with Zr MOFs, Zr MOFs-PEI exhibited a peak at 3300 cm^{-1}, indicating the N-H stretching vibration, which confirmed the successful loading of PEI onto the Zr MOFs. In addition, Figure S2 showed the Zeta potentials of Zr MOFs, PEI and Zr MOFs-PEI, the changes in potential further proved the successful loading of PEI, which established the foundation for the subsequent construction of the ECL aptamer sensor. The results conclusively verified the successful preparation of Zr MOFs and Zr MOFs-PEI composite.

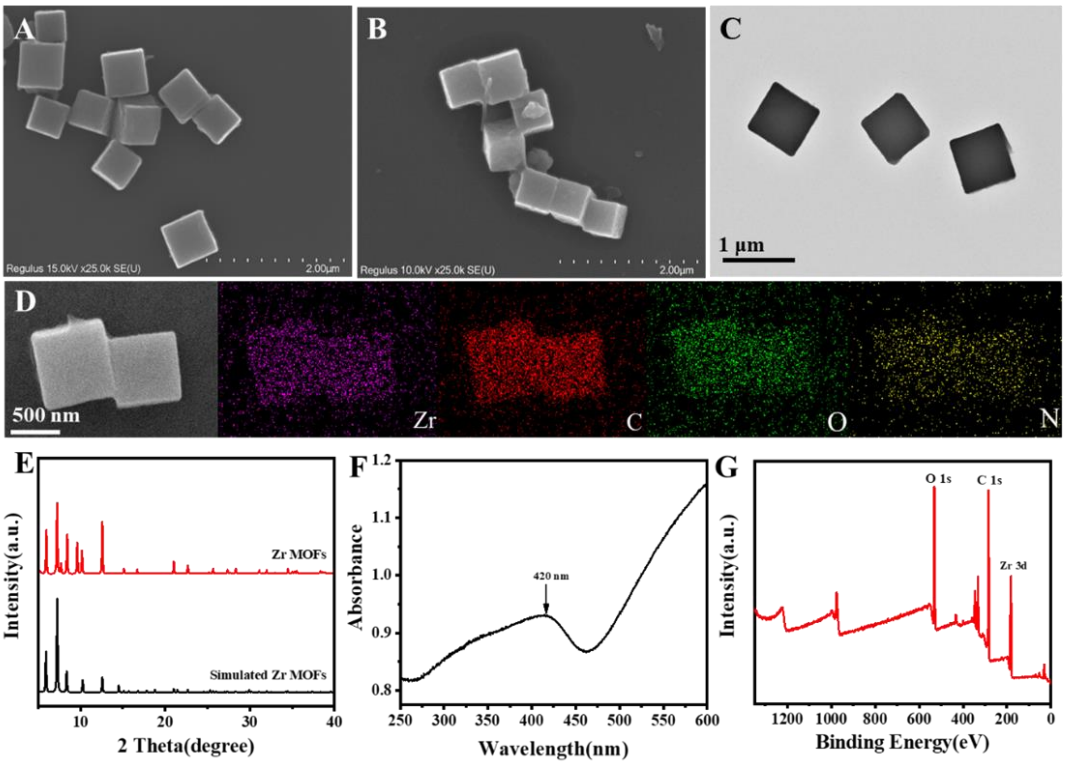

 doi:10.20944/preprints202504.0813.v1

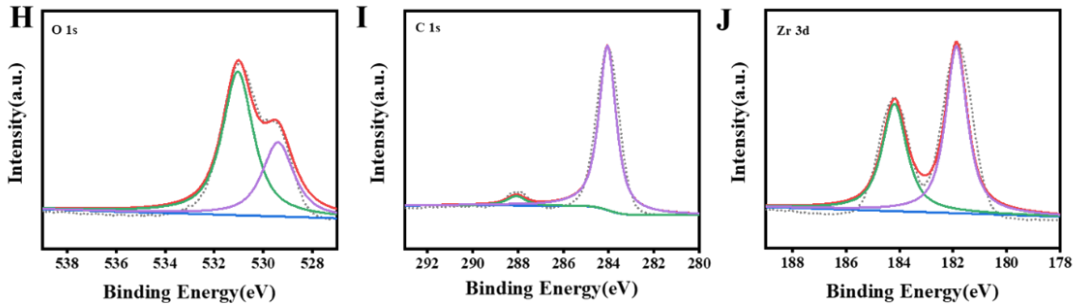

Figure 1. (A) SEM image of Zr MOFs. SEM image (B), TEM image (C) and Element mapping images (D) of Zr MOFs-PEI. XRD pattern (E) and UV-vis spectrum (F) of Zr MOFs. (G) XPS survey spectrum and high-resolution spectra of (H) O 1s, (I) C 1s and (J) Zr 3d for Zr MOFs.

3.2. Performance of the ECL Self-Enhancement and Competition Mechanism

The emission efficiency of ECL emitters plays a crucial role in improving sensor sensitivity. To boost the ECL signal, PEI was covalently conjugated with the Zr MOFs luminophore to create composite. Through intermolecular interaction, the electron transfer distance was shortened and energy loss minimized, leading to self-enhanced ECL. As depicted in Figure 2A, the bare GCE (curve a) and Zr MOFs (curve b) exhibited negligible ECL signals in PBS solution. However, upon the addition of PEI to the PBS solution containing Zr MOFs (curve c), a significant enhancement in the ECL signal was observed. Notably, the ECL signal of Zr MOFs-PEI in PBS (curve d) was enhanced by approximately 5.8 times compared to that of Zr MOFs alone in PBS containing PEI. This remarkable enhancement, attributed to the intermolecular self-enhancement effects of Zr MOFs-PEI, renders it an excellent high-intensity emitter for the development of a dual-signal competitive ECL aptamer sensor.

Furthermore, the distinct lack of spectral overlap between the ECL spectrum of Zr MOFs (curve a) and the UV-vis absorption spectrum of Luminol (curve b), as depicted in Figure 2B, was a noteworthy observation. This suggests that in the competitive dual-signal ECL aptamer sensor, the reduction of the Zr MOFs signal upon the introduction of Luminol is primarily attributed to the competition for the co-reactant PEI, rather than resonance energy transfer. This key finding underscored the significance of eliminating potential interference of resonance energy transfer phenomena, and establishing an accurate quantitative relationship in the competitive dual-signal ECL aptamer sensor.

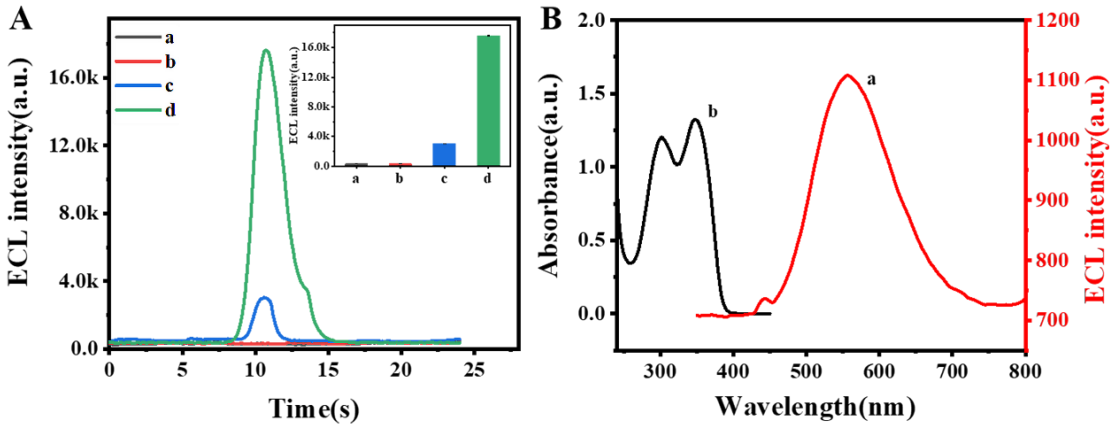

Figure 2. (A) ECL signals of (a) bare GCE, (b) Zr MOFs, (c) mixture of Zr MOFs and PEI, (d) Zr MOFs-PEI in PBS. (B) ECL spectrum of Zr MOFs-PEI (a) and UV-visible absorption spectrum of Luminol (b).

 doi:10.20944/preprints202504.0813.v1

Subsequently, the synergistic mechanism of self-enhancing ECL strategy and single co-reactant competition was deeply analyzed, as shown in Figure 3. The corresponding reaction equations were presented to explain the generation and enhancement of the ECL signals.

$$\text{Zr MOFs-PEI} - 2e^- \longrightarrow \text{Zr MOFs}^+\text{-PEI}^{\cdot+} \quad (1)$$

$$\text{Zr MOFs}^+\text{-PEI}^{\cdot+} \longrightarrow \text{Zr MOFs}^+\text{-PEI}^{\cdot} + H^+ \quad (2)$$

$$\text{Zr MOFs}^+\text{-PEI}^{\cdot} \longrightarrow \text{Zr MOFs}^*\text{-PEI} + H^+ \quad (3)$$

$$\text{Zr MOFs}^*\text{-PEI} \longrightarrow \text{Zr MOFs-PEI} + h\nu_1 \quad (4)$$

$$\text{Luminol} - 2e^- - 2H^+ \longrightarrow \text{Luminol}^{\cdot-} \quad (5)$$

$$\text{Luminol}^{\cdot-} + \text{Zr MOFs}^+\text{-PEI}^{\cdot+} \longrightarrow \text{Luminol}^* + \text{Products} \quad (6)$$

$$\text{Luminol}^* \longrightarrow \text{Luminol} + h\nu_2 \quad (7)$$

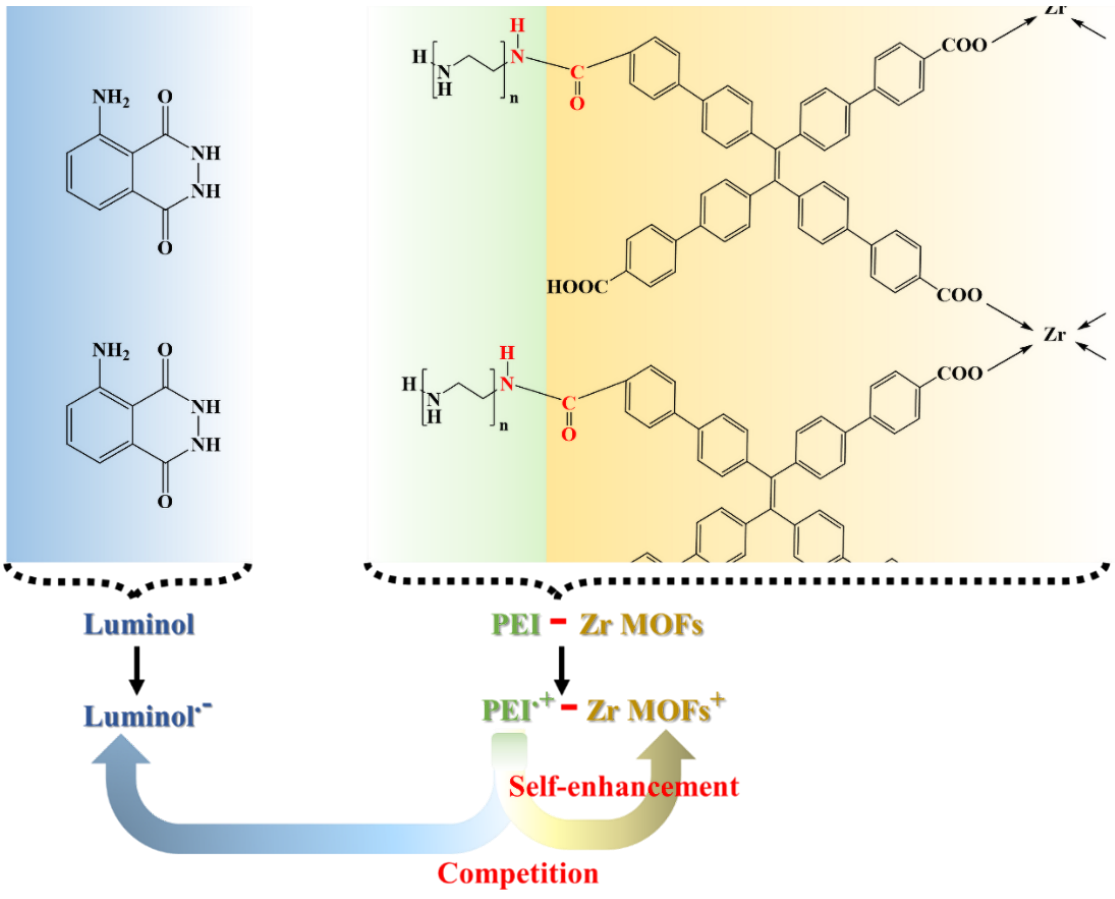

Figure 3. Proposed synergistic mechanism of self-enhanced ECL strategy and single co-reactant competition.

3.3. Electrochemical Characterization and ECL Behavior

To explore the assembly process of the ECL aptasensor, cyclic voltammetry (CV) and electrochemical impedance spectroscopy (EIS) were utilized to study the electrochemical properties. As shown in Figure 4A, the bare GCE exhibited a pair of reversible oxidation-reduction peaks (curve a). Upon modification with Zr MOFs-PEI, the peak current was observed to decrease (curve b).

 doi:10.20944/preprints202504.0813.v1

Following the addition of the aptamer for KAN, the peak current exhibited further reduction (curve c). The subsequent binding of KAN to the aptamer significantly lowered the peak current (curve d). Finally, upon modification with the Luminol-Apt probe, the peak current experienced another decrement (curve e). The EIS spectra in Figure 4B showed a gradual increase in the electron transfer resistance (*Ret*) value at each step of the modified electrode (curves a ~ e), thus confirming the successful fabrication of the ECL aptamer sensor.

As shown in Figure 4C, the ECL behavior of the sensor was characterized subsequently. Compared with the bare GCE (curve a), the modification of Zr MOFs-PEI produced a pronounced ECL signal (curve b). Clearly visible from the inset, the ECL signals of Zr MOFs remained stable after binding with the aptamer (curve c) and capturing KAN (curve d), which proved that the modification of the aptamer and KAN had no effect on the luminescence properties of Zr MOFs. After the introduction of the Luminol-Apt, the competition for the PEI resulted in an enhanced ECL signal of Luminol and a diminished signal of Zr MOFs (curve e). This result further validated the successful preparation of the competitive dual-signal ECL aptamer sensor.

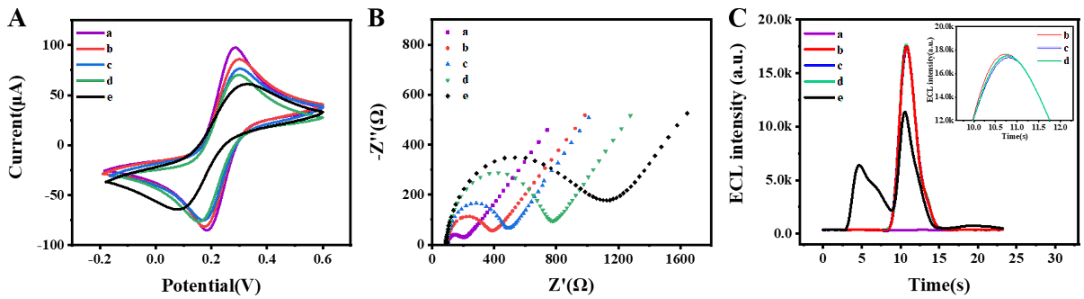

Figure 4. (A) CV and (B) EIS characterization of the ECL aptamer sensor in 0.1 M KCl solution containing 5.0 mM $[Fe(CN)_6]^{3-/4-}$. (C) ECL curves of (a) bare GCE, (b) Zr MOFs-PEI/GCE, (c) Apt/Zr MOFs-PEI/GCE, (d) KAN/Apt/Zr MOFs-PEI/GCE, (e) Luminol-Apt/KAN/Apt/Zr MOFs-PEI/GCE in PBS, the inset is a partial magnification of curves b ~ d.

3.4. Optimization of the Detection Conditions

To enhance the detection performance of the ECL aptamer sensor, a comprehensive optimization of experimental conditions was carried out. As illustrated in Figure S3, the concentration of Luminol was optimized. As concentration of Luminol increased, the ECL signal of Zr MOFs decreased significantly and remained stable at 12.5 mM, so it was chosen as the optimal concentration of Luminol. Additionally, the adjustment of the incubation time of the Luminol-Apt was shown in Figure S4, it took 150 min for the full binding of Luminol-Apt with KAN. When the reaction time exceeded 150 min, the intensities remained basically stable. Therefore, the subsequent incubation time of the Luminol-Apt was set at 150 min. The optimization of the incubation time for KAN binding to the aptamer was depicted in Figure S5. It was observed that the complete combination of KAN and aptamer occurred within 60 min, with minimal subsequent variation in the intensities. Thus, 60 min was determined to be the optimal reaction time. As shown in Figure S6, within the range of 1.0 nM to 1.0×10^2 nM, the ECL intensity of luminol increased with the increase in the concentration of aptamer. Then, with the further increase, the ECL intensity of both of luminol and Zr MOFs decreased sharply, mainly because excessive aptamer would cover the surface of Zr-MOF-PEI, which hindered the luminescence of Zr-MOF and luminol. Therefore, the most suitable concentration of aptamer for KAN was determined to be 1.0×10^2 nM. The optimal experimental conditions obtained above were paramount in ensuring the reliability and efficiency of the aptasensor in practical applications.

3.5. Analytical Performance

Under the optimized conditions, various concentrations of KAN were detected, and the corresponding ECL signals were plotted in Figure 5A. As depicted in Figure 5B, the ECL intensity

 doi:10.20944/preprints202504.0813.v1

ratio ($I_{Luminol}/I_{Zr\ MOFs}$) between Luminol and Zr MOFs exhibited a linear relationship with the logarithm of KAN concentration ranging from 1.0 × 10^{-3} to 1.0 × 10^{5} ng/mL. The obtained linear regression equation was $I_{Luminol}/I_{Zr\ MOFs} = 0.154 \lg C_{KAN} + 0.547$（$R^2 = 0.998$）. The detection limit (7.86 × 10^{-4} ng/mL) was lower than that reported in previous studies (Table S1), demonstrating that the dual-signal ECL aptamer sensor exhibits excellent analytical performance for KAN detection.

In addition, selectivity and repeatability are considered to be essential parameters for assessing the practicality of the ECL aptamer sensors. Antibiotics such as chloramphenicol (CAP), tetracycline (TET), lincomycin (LIN), ampicillin (AM), and streptomycin (STP) were used to evaluate the selectivity of the constructed ECL aptamer sensor. The selected interferents are typically antibiotics co-existing in milk or other food samples, which may interfere with the detection of KAN in practical applications. As illustrated in Figure 5C, even when the concentrations of these interfering substances were 100-fold higher than that of KAN, they still did not significantly affect the detection of KAN, proving that the ECL aptamer sensor has satisfactory selectivity. To further investigate the repeatability of the ECL sensor, 10 tests were performed for 1 ng/mL KAN under the same experimental conditions (Figure 5D). The repeatability was evaluated by calculating the relative standard deviation (RSD) of 10 independent measurements. The ECL signals were basically stable, the RSD of Zr MOFs was 1.27%, and the RSD of Luminol was 1.78%. Therefore, based on the high selectivity and excellent repeatability, the constructed dual-signal ECL aptamer sensor demonstrates promising potential for practical applications of detecting KAN in complex matrices.

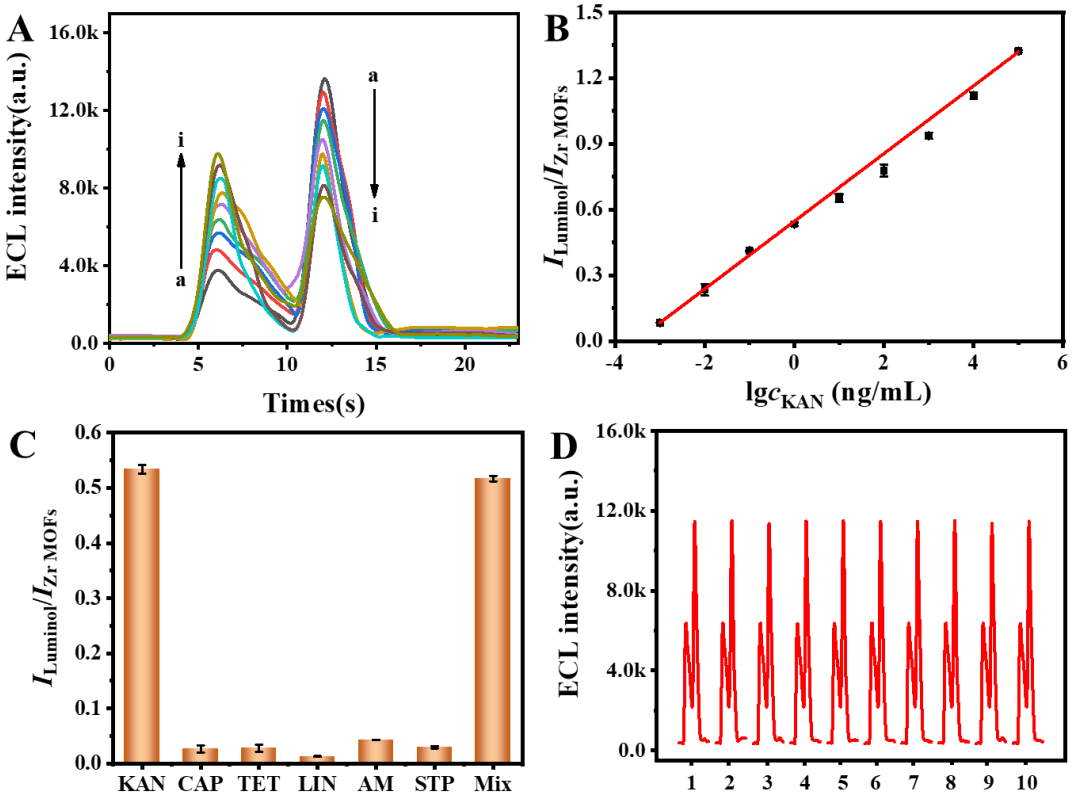

Figure 5. (A) ECL aptamer sensors response of various KAN concentrations from 1.0 × 10^{-3} ng/mL to 1.0 × 10^{5} ng/mL. (B) Calibration curve of the ECL aptamer sensor for the detection of KAN. (C) Selectivity (1.0 and 1.0 × 10^{2} ng/mL for KAN and other interfering analytes, respectively) and (D) repeatability of the ECL aptamer sensor.

3.6. Real Sample Analysis

To verify the practicability of the designed competitive dual-signal ECL aptamer sensors, KAN levels in various samples were assessed using the standard addition method to simulate complex

 doi:10.20944/preprints202504.0813.v1

substrates found in food and environmental samples. The pretreatment of the real samples is shown in Supplementary Material. As depicted in Table 1, recoveries ranged from 97.1% to 104.0%, and the RSD of the ECL sensors was less than 2.9%. The results demonstrated that the ECL aptamer sensor exhibited reliability in the real sample analysis.

Table 1. Recoveries for the detection of KAN.

Sample	Spiked (ng/mL)	Found (ng/mL)	Recovery (%)	RSD(%)
Milk	0	No Found	-	-
	0.01	0.01	100	0.4
	1.00	1.00	100	1.1
	100.0	102.6	103	1.1
River water	0	No Found	-	-
	0.01	0.01	100	2.9
	1.00	1.03	103	2.2
	100.0	97.11	97.1	1.0
Honey	0	No Found	-	-
	0.01	0.01	100	1.2
	1.00	1.04	104	1.5
	100.0	98.78	98.8	0.5

4. Conclusions

In summary, based on the competition between Zr MOFs with self-enhancing effects and Luminol for the single co-reactant PEI, we have devised a novel dual-signal ECL sensing platform for highly sensitive detection of KAN. The exceptional performance of this platform could be attributed to several critical factors. Firstly, the covalent binding of Zr MOFs and PEI was conducive to reducing the electron transfer distance and minimizing the energy loss, thus effectively enhancing the ECL signal intensity and boosting the sensitivity. Secondly, the abundant active sites in Zr MOFs facilitated the immobilization of aptamer, leading to a higher loading of Luminol signal probe and further enhancing sensitivity. Thirdly, the competition between Zr MOFs and Luminol for PEI introduced a dual-signal self-calibration mode, improving the precision of KAN detection. This work offered a new perspective on the synergistic mechanisms involving self-enhanced ECL and competitive ECL, and opened a new approach for the rational design of dual-signal ECL sensing platforms.

Supplementary Materials: The following supporting information can be downloaded at the website of this paper posted on Preprints.org.

Author Contributions: Conceptualization, Z.H.W.; methodology, Y.W.Z. and X.M.W.; investigation, Y.W.Z. and X.M.W.; data curation, Y.W.Z. and X.M.W.; writing-original draft preparation, Y.W.Z. and X.M.W.; writing—review and editing, X.M.W., Z.Y.Y., F.F.Z., J.F.X., L.L.L. and Z.H.W.; funding acquisition, Z.Y.Y., F.F.Z., J.F.X., L.L.L. and Z.H.W. All authors have read and agreed to the published version of the manuscript.

Funding: This research was funded by the National Natural Science Foundation of China (No.22304013, No. 52203119), the Natural Science Foundation of Shandong Province (ZR2020MB063, ZR2021MB069, ZR2020MB060), the Taishan Scholar Program of Shandong Province (ts201511027), China.

Institutional Review Board Statement: Not applicable.

 doi:10.20944/preprints202504.0813.v1

Informed Consent Statement: Informed consent was obtained from all subjects involved in the study.

Data Availability Statement: The experimental data is contained within the article.

Acknowledgments: This work was financially supported by the National Natural Science Foundation of China (No.22304013, No.52203119), the Natural Science Foundation of Shandong Province (ZR2020MB063, ZR2021MB069, ZR2020MB060), the Taishan Scholar Program of Shandong Province (ts201511027), China. The authors thank Dr. Wang Huiqi, Dr. Cao Xiyue and Dr. Li Ru from Instrumental Analysis Center of Qingdao University for their help in material measurements.

Conflicts of Interest: The authors declare no conflict of interest.

References

1. Heysell, SK.; Ahmed, S.; Rahman, MT. Hearing loss with kanamycin treatment for multidrug−resistant tuberculosis in Bangladesh. *Eur. Respir. J* **2018**, *51*, 1701778. https://doi.org/10.1183/13993003.01778-2017
2. Brezden, A.; Mohamed, M.F.; Nepal, M.; Harwood, J.S.; Kuriakose, J.; Seleem, M.N.; Chmielewski, J. Correction to "dual targeting of intracellular pathogenic bacteria with a cleavable conjugate of kanamycin and an antibacterial cell-penetrating peptide". *J. Am. Chem. Soc* **2016**, *138*, 10945−10949. https://doi.org/10.1021/jacs.8b09906
3. Wang, C.; Li, Y.J.; Zhu, Y.B.; Zhou, X.H.; Lin, Q.; He, M. High−κ solid-gate transistor configured graphene biosensor with fully integrated structure and enhanced sensitivity. *Adv. Funct. Mater* **2016**, *26*, 7668−7678. https://doi.org/10.1002/adfm.201602960
4. Habeeb Rahman A.P.; Pranjal; Behera, S.K.; Mishra, A.; Lundborg, C.S.; Tripathy, S.K. Transcriptomic regulation of Salmonella Typhimurium during sonophotocatalysis and the effect of stress adaptation on the antibiotic resistance and tolerance post−treatment. *Chem. Eng. J* **2022**, *446*, 137442. https://doi.org/10.1016/j.cej.2022.137442
5. Chen, Z.H.; Liu, X.; Chen, L.W.; Han, Y.; Shen, Y.M.; Chen, B.L.; Wang, M.Z. Deglycosylation inactivation initiated by a novel periplasmic dehydrogenase complex provides a novel strategy for eliminating the recalcitrant antibiotic kanamycin. *Environ. Sci. Technol* **2023**, *57*, 4298−4307. https://doi.org/10.1021/acs.est.2c09565
6. Guo, Z.; He, J.X.; Mahadevegowda, S.H.; Kho, S.H.; Chan-Park, M.B.; Liu, X.W. Multifunctional glyco−nanosheets to eradicate drug-resistant bacteria on wounds. *Adv. Healthc. Mater* **2020**, *9*, 2000265. https://doi.org/10.1002/adhm.202000265
7. Wang, C.S.; Liu, C.; Luo, J.B.; Tian, Y.P.; Zhou, N.D. Direct electrochemical detection of kanamycin based on peroxidase-like activity of gold nanoparticles. *Anal. Chim. Acta* **2016**, *936*, 75-82. https://doi.org/10.1016/j.aca.2016.07.013
8. Wang, W.Z.; Gunasekaran, S. Oxygen-terminated few−layered Ti_3C_2Tx MXene nanosheets as peroxidase−mimic nanozyme for colorimetric detection of kanamycin. *Biosens. Bioelectron* **2022**, *218*, 114774. https://doi.org/10.1016/j.bios.2022.114774
9. Zhao, T.T.; Chen, Q.; Wen, Y.L.; Bian, X.J.; Tao, Q.; Liu, G.; Yan, J. A competitive colorimetric aptasensor for simple and sensitive detection of kanamycin based on terminal deoxynucleotidyl transferase-mediated signal amplification strategy. *Food Chem* **2022**, *377*, 132072. https://doi.org/10.1016/j.foodchem.2022.132072
10. He, Y.H.; Wen, X.Y.; Zhang, B.Y.; Fan, Z.F. Novel aptasensor for the ultrasensitive detection of kanamycin based on graphene oxide quantum−dot−linked single−stranded DNA−binding protein. *Sens. Actuators B Chem* **2018**, *265*, 20-26. https://doi.org/10.1016/j.snb.2018.03.029
11. Wang, X.Y.; Zhang, W.Q.; Gao, X.L.; Sun, Z.C.; Sun, X.; Guo, Y.M.; Li, F.L.; Boboriko, N.E. Fluorescent aptasensor based on DNA−AgNCs emitting in the visible red wavelength range for detection of kanamycin in milk. *Sens. Actuators B Chem* **2022**, *360*, 131665. https://doi.org/10.1016/j.snb.2022.131665
12. Wang, C.S.; Liu, J.; Han, X.Y.; Liu, C.; Tian, Y.P.; Zhou, N.D. UV-visible spectroscopic detection of kanamycin based on target−induced growth of gold nanoparticles. *Anal. Methods* **2017**, *9*, 4843. https://doi.org/10.1039/C7AY01685A

 doi:10.20944/preprints202504.0813.v1

13. Zhong, C.Z.; Zhang, C.Z.; Yang, Y.; Liang, X.X.; Pang, Q.; Zhou, L.Y.; Chen, P.C. Synergistic effect of photoelectrochemical aptasensor based on staggered gap ZnO/$BiFeO_3$ heterojunction coupled with cDNA−CdS sensitizer enabling ultrasensitive assay of kanamycin. *Food Chem* **2024**, *437*, 137877. https://doi.org/10.1016/j.foodchem.2023.137877
14. Cheng, S.T.; Liu, H.M.; Zhang, H.; Chu, G.L.; Guo, Y.M.; Sun, X. Ultrasensitive electrochemiluminescence aptasensor for kanamycin detection based on silver nanoparticle−catalyzed chemiluminescent reaction between luminol and hydrogen peroxide. *Sens. Actuators B Chem* **2020**, *304*, 127367. https://doi.org/10.1016/j.snb.2019.127367
15. Gao, X.L.; Sun, Z.C.; Wang, X.Y.; Zhang, W.Q.; Xu, D.Y.; Sun, X.; Guo, Y.M.; Xu, S.C.; Li, F.L. Construction of a dual-model aptasensor based on G-quadruplexes generated via rolling circle amplification for visual/sensitive detection of kanamycin. *Sci. Total Environ* **2022**, *839*, 156276. https://doi.org/10.1016/j.scitotenv.2022.156276
16. Zheng, L.; Li, Q.; Deng, X.K.; Guo, Q.F.; Liu, D.D.; Nie, G.M. J, A novel electrochemiluminescence biosensor based on $Ru(bpy)_3^{2+}$−functionalized MOF composites and cycle amplification technology of DNAzyme walker for ultrasensitive detection of kanamycin. *Colloid Interface Sci* **2024**, *659*, 859-867. https://doi.org/10.1016/j.jcis.2024.01.045
17. Zhang, X.; Wang, P.L.; Nie, Y.X.; Ma, Q. Recent development of organic nanoemitter-based ECL sensing application. *TrAC* **2021**, *143*, 116410. https://doi.org/10.1016/j.trac.2021.116410
18. Liao, Y.H.; Fan, Z.J.; Deng, H.P.; Yang, Y.; Li, J.Y.; Zhao, Z.Y.; Tan, Q.Q.; Li, B.; Huang, X. Zika virus liquid biopsy: A dendritic $Ru(bpy)_3^{2+}$−polymer−amplified ECL diagnosis strategy using a drop of blood. *ACS Cent. Sci* **2018**, *4*, 1403−1411. https://doi.org/10.1021/acscentsci.8b00471
19. Du, L.; Zhang, H.X.; Wang, Z.Y.; Zhuang, T.T.; Wang, Z.H. Boosting the electrochemiluminescence of luminol by high-intensity focused ultrasound pretreatment combined with 1T/2H MoS_2 catalysis to construct a sensitive sensing platform. *Ultrason. Sonochem* **2023**, *92*, 106264. https://doi.org/10.1016/j.ultsonch.2022.106264
20. He, Y.; Hu, F. X.; Zhao, J. W.; Yang, G. M.; Zhang, Y. Y.; Chen, S. H.; Yuan, R. Bifunctional moderator-powered ratiometric electrochemiluminescence enzymatic biosensors for detecting organophosphorus pesticides based on dual-signal combined nanoprobes. *Anal. Chem* **2021**, *93*, 8783−8790. https://doi.org/10.1021/acs.analchem.1c00179
21. Tan, Y.Y.; Tan, H.S.; Liu, M.J.; Li, S.S. Electrochemical ratiometric dual−signal immunoassay for accurate detection of carcinoembryonic antigen in clinical serum based on rGO−Pd@Au−Thi and Chi−Fc−Au. *Sens. Actuators B Chem* **2023**, *380*, 133340. https://doi.org/10.1016/j.snb.2023.133340
22. Wang, Y.Z.; Li, Y.R.; Zhang, Y.Q.; Xiang, Y.M.; Bai, R.R.; Liu, Y.; Li, M.L.; Meng, G.R.; Pan, S.L.; Zhang, F.; Mi, L.; Hu, Y.H. Dual−signal ratiometric electrochemiluminescence biosensor based on Au NPs-induced low-potential emission of PFO Pdots and LSPR-ECL mechanism for ultra-sensitive detection of microRNA-141. *Biosens. Bioelectron* **2024**, *261*, 116495. https://doi.org/10.1016/j.bios.2024.116495
23. Zhang, W.; Cui, X.M.; Li, F.H.; Yan, W.; Wang, Y.Y.; Shang, L.; Ma, R.N.; Jia, L.P.; Li, C.; Wang, H.S. Perylene diimide and g−C_3N_4 nanosheet as potential-resolved cathode luminophores for ultrasensitive ratiometric electrochemiluminescence immunosensor. *Sens. Actuators B Chem* **2022**, *371*, 132492. https://doi.org/10.1016/j.snb.2022.132492
24. Dai, W. J.; Chen, G. X.; Wang, X. Y.; Zhen, S. J.; Huang, C. Z.; Zhan, L.; Li, Y. F. Facile synthesis of dual-ligand europium-metal organic gels for ratiometric electrochemiluminescence detecting I27L gene. *Biosens. Bioelectron* **2024**, *246*, 115863. https://doi.org/10.1016/j.bios.2023.115863
25. Chen, G.X.; Hu, C.Y.; Dai, W.J.; Luo, Z.L.; Zang, H.; Sun, S.Y.; Zhen, S.J.; Zhan, L.; Huang, C.Z.; Li, Y.F. Coreactant-free zirconium metal−organic framework with dual emission for ratiometric electrochemiluminescence detection of HIV DNA. *Anal. Chem* **2024**, *96*, 10102-10110. https://doi.org/10.1021/acs.analchem.4c02187
26. Wang, X.M.; Hou, C.T.; Zhang, F.F.; Xia, J.F.; Wang, Z.H. Highly sensitive electrochemiluminescence biosensor based on novel TiO_2−porphyrin organic framework with self−enhanced luminescent property. *Sens. Actuators B Chem* **2023**, *379*, 133229. https://doi.org/10.1016/j.snb.2022.133229

 doi:10.20944/preprints202504.0813.v1

27. Zhao, Y.Q.; Zhao, A.J.; Wang, Z.Z.; Xu, Y.H.; Feng, Y.J.; Lan, Y.B.; Han, Z.G.; Lu, X.Q. Enhancing the electrochemiluminescence of porphyrin via crystalline networks of metal−organic frameworks for sensitive detection of cardiac troponin I. *Anal. Chem* **2023**, *95*, 11687-11694. https://doi.org/10.1021/acs.analchem.3c01647
28. Zhao, L. Y.; Zhao, H. Q.; Shang, L., Shen, G. D.; Ma, R. N.; Wang, H. S. A robust ECL-enhanced system based on UiO-66-COOH promoting perylene diimide derivative electrochemiluminescence for tumor biomarker detection. *Sens. Actuators B Chem* **2025**, *423*, 136824. https://doi.org/10.1016/j.snb.2024.136824
29. Li, Y.; Dong, X.; Wu, T. T.; Zhang, X. Y.; Ren, X.; Feng, R.; Du, Y.; Lee, J. Y.; Liu, X. T.; Wei, Q. Zirconium based metal–organic frameworks with aggregation-induced electrochemiluminescence for sensitive analysis of aflatoxin B1 by signal dual-amplification strategy. *Chem. Eng. J* **2024**, *500*, 157308. https://doi.org/10.1016/j.cej.2024.157308
30. Bushira, F.A.; Hussain, A.; Wang, P.; Li, H.J.; Zheng, L.R.; Gao, Z.Q.; Dong, H.F.; Jin, Y.D. Boosting electrochemiluminescence performance of a dual-active site iron single-atom catalyst-based luminol–dissolved oxygen system via plasmon-induced hot holes. *Anal. Chem* **2024**, *96*, 9704-9712. https://doi.org/10.1021/acs.analchem.4c01744
31. Chen, X.D.; Xv, H.J.; Li, C.; Kong, L.H.; Li, C.X.; Li, F. Fe-single-atom catalysts boosting electrochemiluminescence via bipolar electrode integrated with its peroxidase-like activity for bioanalysis. *Biosens. Bioelectron* **2024**, *258*, 116351. https://doi.org/10.1016/j.bios.2024.116351
32. Zhou, X.Y.; Zou, Y.Q.; Ru, H.J.; Yan, F.; Liu, J.Y. Silica nanochannels as nanoreactors for the confined synthesis of Ag NPs to boost electrochemical stripping chemiluminescence of the luminol-O_2 system for the sensitive aptasensor. *Anal. Chem* **2024**, *96*, 10264-10273. https://doi.org/10.1021/acs.analchem.4c01033
33. Wei, Z.W.; Gu, Z.Y.; Arvapally, R.K.; Chen, Y.P.; Jr, R.M.; Ivy, J.F.; Yakovenko, A.A.; Feng, D.W.; Omary, M.A.; Zhou, H.C. Rigidifying fluorescent linkers by metal−organic framework formation for fluorescence blue shift and quantum yield enhancement. *J. Am. Chem. Soc* **2014**, *136*, 8269−8276. https://doi.org/10.1021/ja5006866